The Plant Cell, Vol. 26: 1134–1150, March 2014, www.plantcell.org

Strigolactone Promotes Degradation of DWARF14, an α/β Hydrolase Essential for Strigolactone Signaling in *Arabidopsis*[W]

Florian Chevalier,[a] Kaisa Nieminen,[b,1] Juan Carlos Sánchez-Ferrero,[c,2] María Luisa Rodríguez,[a,3] Mónica Chagoyen,[c] Christian S. Hardtke,[b] and Pilar Cubas[a,4]

[a] Plant Molecular Genetics Department, Centro Nacional de Biotecnología/Consejo Superior de Investigaciones Científicas, Campus Universidad Autónoma de Madrid, 28049 Madrid, Spain

[b] Department of Plant Molecular Biology, University of Lausanne, CH-1015 Lausanne, Switzerland

[c] Computational Systems Biology Group, Centro Nacional de Biotecnología/Consejo Superior de Investigaciones Científicas, Campus Universidad Autónoma de Madrid, 28049 Madrid, Spain

Strigolactones (SLs) are phytohormones that play a central role in regulating shoot branching. SL perception and signaling involves the F-box protein MAX2 and the hydrolase DWARF14 (D14), proposed to act as an SL receptor. We used strong loss-of-function alleles of the *Arabidopsis thaliana D14* gene to characterize *D14* function from early axillary bud development through to lateral shoot outgrowth and demonstrated a role of this gene in the control of flowering time. Our data show that D14 distribution in vivo overlaps with that reported for MAX2 at both the tissue and subcellular levels, allowing physical interactions between these proteins. Our grafting studies indicate that neither *D14* mRNA nor the protein move over a long range upwards in the plant. Like MAX2, D14 is required locally in the aerial part of the plant to suppress shoot branching. We also identified a mechanism of SL-induced, *MAX2*-dependent proteasome-mediated degradation of D14. This negative feedback loop would cause a substantial drop in SL perception, which would effectively limit SL signaling duration and intensity.

INTRODUCTION

Plant architecture is determined in great part by branching patterns. Branches develop from axillary meristems (AMs) that form at the base of leaves. AMs undergo a growth period during which they initiate leaf primordia (and sometimes flower meristems) with no internode elongation and give rise to axillary buds. These buds can be developmentally arrested for long time periods or continue to grow to generate lateral shoots. The great diversity of branching patterns among flowering plants is determined both by the arrangement of leaves in the stem (phyllotaxis), where axillary buds are formed, and by the decision of buds to grow out to give rise to a branch or remain dormant. Phyllotaxis is mostly unaffected by external cues, whereas axillary bud outgrowth shows great plasticity, as it is regulated by developmental and environmental stimuli, such as apical dominance, nutrient availability, and light quality.

Study of the genetic pathways that regulate branch development shows a large degree of conservation over a wide range of angiosperm species, such as maize (*Zea mays*), rice (*Oryza sativa*), petunia (*Petunia hybrida*), tomato (*Solanum lycopersicum*), pea (*Pisum sativum*), and thale cress (*Arabidopsis thaliana*). Genetic and regulatory divergence have nonetheless been found (Drummond et al., 2011; Delaux et al., 2012; Challis et al., 2013), which could help to account for the variations in branching patterns between groups. In all species analyzed, long-distance signaling and local gene activity participate in the regulation of axillary bud growth. Systemic signaling that prevents branch outgrowth involves auxin and the recently identified hormone strigolactone (SL; Gomez-Roldan et al., 2008; Umehara et al., 2008).

Auxin is synthesized in the shoot apex and transported basipetally (toward the root) through the polar auxin transport stream (PATS) (Thimann and Skoog, 1933; Skoog and Thimann, 1934). SL is synthesized in the root and other plant organs and is transported acropetally (toward the shoot) in the xylem (Foo et al., 2001; Kohlen et al., 2011). Auxin is thought to suppress branching indirectly through two mechanisms, by modulating the activity of second messengers (i.e., SL and cytokinin; Nordström et al., 2004; Brewer et al., 2009) and due to competition between shoot apices for auxin export into the PATS (Domagalska and Leyser, 2011). SL is also proposed to have two roles in the regulation of shoot branching, including dampening of auxin transport, thus enhancing competition between buds for their common auxin sink (Bennett et al., 2006; Prusinkiewicz et al., 2009; Crawford et al., 2010; Balla et al., 2011; Shinohara et al., 2013), and transcriptional activation of the growth repressor *BRANCHED1* (*BRC1*) (Braun et al., 2012; Dun et al., 2012, 2013). *BRC1*-like genes, expressed inside axillary buds, encode class II TCP (for *TEOSINTE BRANCHED1*, *CYCLOIDEA*, and *PCF*) transcription factors (Martín-Trillo and

[1] Current address: Finnish Forest Research Institute, Vantaa Research Unit, Jokiniemenkuja 1, FI-01301 Vantaa, Finland.

[2] Current address: Phenomics and Bioinformatics Research Centre, School of Information Technology and Mathematical Sciences, University of South Australia, Mawson Lakes SA 5095, Australia.

[3] Current address: Technology Division (Chemistry), Repsol Technology Center, Ctra. de Extremadura, A-5, km 18, 28935 Móstoles, Spain.

[4] Address correspondence to pcubas@cnb.csic.es.

The author responsible for distribution of materials integral to the findings presented in this article in accordance with the policy described in the Instructions for Authors (www.plantcell.org) is: Pilar Cubas (pcubas@cnb.csic.es).

[W] Online version contains Web-only data.

www.plantcell.org/cgi/doi/10.1105/tpc.114.122903

Cubas, 2010) that delay bud growth and development and promote bud dormancy (Aguilar-Martínez et al., 2007; Finlayson, 2007; Martín-Trillo et al., 2011; Braun et al., 2012; Dun et al., 2012; González-Grandío et al., 2013).

Several genes involved in SL synthesis and perception, whose mutants show increased branching and reduced stature, have been characterized in a number of species. Active SL is synthesized from β-carotene by a set of proteins conserved in mono- and dicotyledons. The *DWARF27* (*D27*) gene, first characterized in rice, encodes an isomerase that acts at the initial steps of this pathway by transforming *trans*-β-carotene to 9-cis-β-carotene (Lin et al., 2009; Alder et al., 2012; Waters et al., 2012a). CAROTENOID CLEAVAGE DIOXYGENASE7 (CCD7) and CCD8 (HTD1/D17/DAD3/RMS5/MAX3 and D10/DAD1/RMS1/MAX4, respectively) (Sorefan et al., 2003; Booker et al., 2005; Snowden et al., 2005; Johnson et al., 2006; Zou et al., 2006; Arite et al., 2007; Drummond et al., 2009; Pasare et al., 2013) produce carlactone, a putative intermediate compound in the pathway (Alder et al., 2012; Seto et al., 2014). The *MORE AXILLARY GROWTH1* (*MAX1*) gene, so far identified only in *Arabidopsis*, encodes a cytochrome P450 monooxygenase that acts downstream of CCD7 and CCD8 (Booker et al., 2005). The phenotype of excessive branching in mutants for all these SL synthesis genes can be rescued by application of SL.

A second group of genes whose mutants are at least partially insensitive to SL are thought to be involved in SL perception and signaling. *MAX2* genes (Stirnberg et al., 2002; Ishikawa et al., 2005; Johnson et al., 2006) encode F-box proteins that participate in SCF (for Skp1, Cullin, RBX1, F-box protein) complexes of E3 ubiquitin ligases. *D14/DECREASED APICAL DOMINANCE2/HTD2* (*D14/DAD2/HTD2*) code for α/β-fold hydrolases that bind and hydrolyze SL in vitro (Arite et al., 2009; Gao et al., 2009; Liu et al., 2009; Gaiji et al., 2012; Hamiaux et al., 2012; Waters et al., 2012b; Kagiyama et al., 2013; Nakamura et al., 2013). In yeast two-hybrid assays, the petunia DAD2 and MAX2b proteins interact in an SL concentration–dependent manner (Hamiaux et al., 2012). This interaction has been confirmed in rice for D14 and D3 (Jiang et al., 2013; Zhou et al., 2013). These findings have led to the proposal that DAD2/D14 is the SL receptor that, after interaction with SL, binds MAX2/D3 to select target proteins for degradation. Rice proteins D53 and SLENDER RICE1 (SLR1) (Jiang et al., 2013; Zhou et al., 2013; Nakamura et al., 2013) and *Arabidopsis* BRI1-EMS-SUPPRESSOR1 (BES1) (Wang et al., 2013) are likely targets for degradation through this pathway. A protein closely related to D14/DAD2, D14-like/KARRIKIN-INSENSITIVE2 (KAI2), genetically interacts with MAX2 (Waters et al., 2012b). KAI2 binds a second hormone, karrikin (KAR), a compound present in bushfire smoke that triggers seed germination (Bythell-Douglas et al., 2013; Guo et al., 2013b; Kagiyama et al., 2013). These observations suggested that D14 and KAI2 mediate SL and KAR signaling, respectively, through interaction with MAX2 (Waters et al., 2012b, 2013).

In this study, we screened for mutants with excessive branching at high-planting density and identified *seto5*, an allele of the *Arabidopsis D14* gene. *Seto5* carries a point mutation in a conserved residue of the protein that reveals an amino acid position essential for D14 function. We compared *D14* promoter activity and D14 protein distribution and found that they are not identical, which might indicate that D14 moves between cells within a short range. Nonetheless, it cannot move acropetally from the root to rescue the shoot branching phenotype of *d14* mutants. Most notably, we discovered a mechanism of negative feedback regulation by which SL induces rapid degradation of D14, which could effectively limit the duration and intensity of SL signaling.

RESULTS

Identification and Phenotypic Characterization of the *seto5* Mutant

To identify genes involved in the regulation of shoot branching, we performed a genetic screen to search for mutants with increased numbers of lateral shoots. We grew ethyl methanesulfonate–mutagenized Columbia-0 (Col-0) plants at a density of nine plants/36 cm^2 pot, a condition that leads to complete branch suppression in wild-type plants (Aguilar-Martínez et al., 2007). We screened for individuals with four or more lateral branches and termed them *seto* (*bush* in Spanish) mutants. One plant bred true (*seto5*), yielding plants that consistently displayed a bushy phenotype. We backcrossed *seto5* to wild-type Col-0 plants and confirmed 3:1 wild type:mutant segregation in the F2 population, indicating that a single locus is responsible for the phenotype.

seto5 mutants, backcrossed twice to Col-0, had a significantly larger number of primary rosette branches (RI, Figure 1) than the wild type (Figures 1B and 1C). In growth conditions in which wild-type plants had approximately two primary rosette branches at maturity, mutants had more than six primary rosette branches. *seto5* plants had fewer secondary branches (RII and CII, Figure 1A) relative to primary branch number (Figure 1D). In addition, mutant plants were slightly shorter than controls (Figure 1E).

To study the *seto5* mutant phenotype during early bud development, we compared the developmental stage of wild-type and *seto5* axillary buds formed at identical node positions in plants grown for 28 d in long photoperiods. At this stage, all plants had undergone flowering and were starting to bolt. In wild-type plants, buds nearest the apex were more developmentally advanced than those farther from the apex (Figure 1F, top). This gradient was also observed in *seto5* mutants, but all buds were developmentally more advanced than those of the wild type (Figure 1F, bottom).

To determine whether flowering time of lateral inflorescences was also accelerated, we counted, in lateral shoots, the number of leaves formed before emergence of the first flower. In wild-type and *seto5* plants, we studied the branch formed in the most apical rosette leaf (−1) and those in the two most basal cauline leaves (+1 and +2) (Figure 1G). *seto5* mutant lateral inflorescences had one fewer leaf than the wild type, as reported for mutants in the *BRC1* locus (Niwa et al., 2013; Figure 1G). Double mutant *seto5 brc1-2* plants resembled *brc1-2* mutants, indicating that *brc1-2* is epistatic for this character (Figure 1G).

These results suggest that, in wild-type plants, the *SETO5* locus delays axillary bud development, lateral shoot outgrowth, and flowering time of lateral inflorescences.

Cloning of *seto5*

High-resolution mapping (Supplemental Figure 1) combined with whole-genome sequencing of *seto5* individuals allowed the identification of a single homozygous nonsynonymous nucleotide

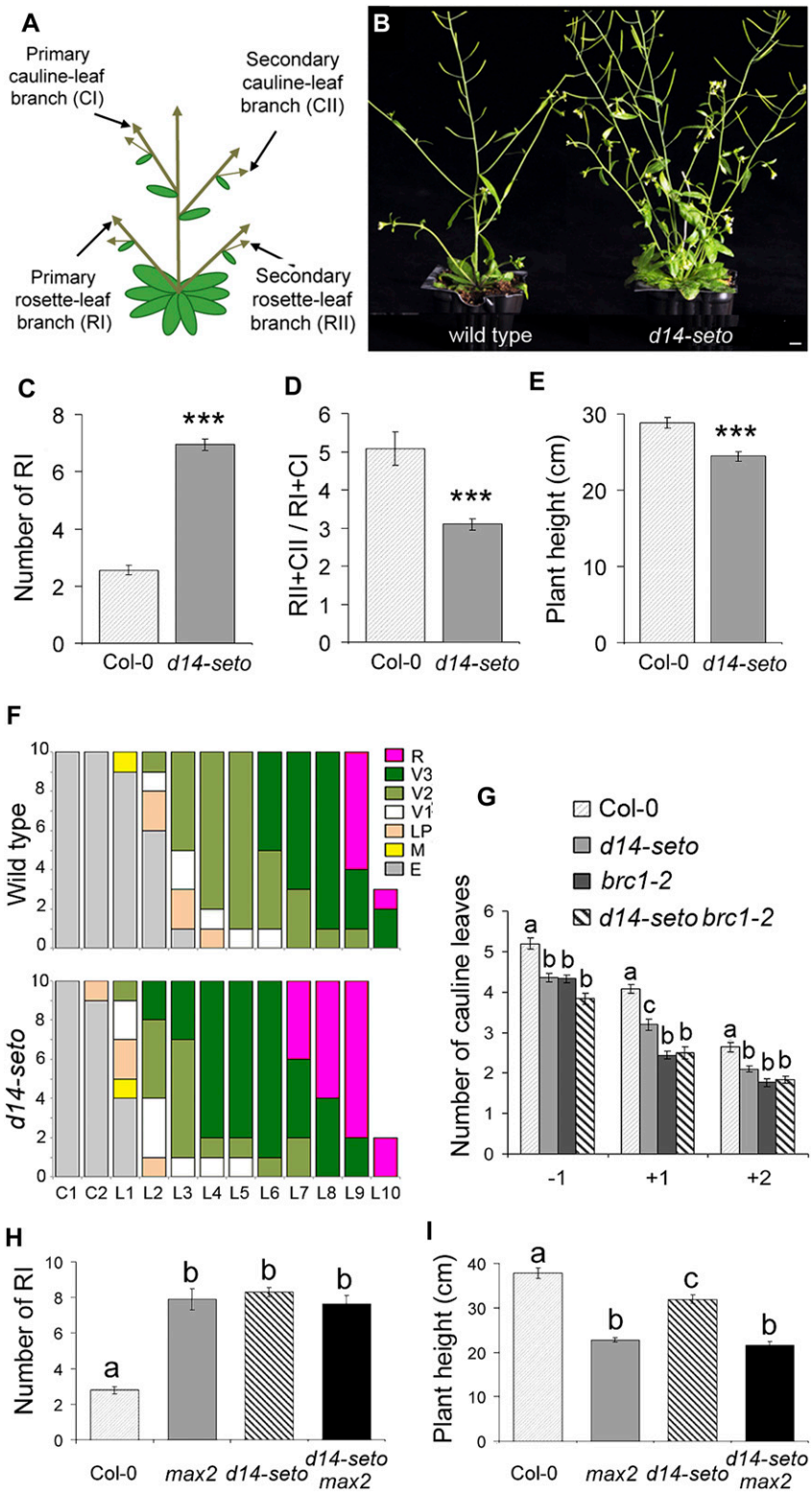

Figure 1. Phenotypes of *d14-seto* Single and Double mutants.

(A) *Arabidopsis* branching structure.
(B) Close-up of mature wild-type Col-0 (left) and *seto5* (here termed *d14-seto*) (right) rosettes showing their lateral shoot phenotype. Bar = 1 cm.

substitution localized within the 163-kb interval of chromosome 3 that included *seto5*. It affected the At3g03990 gene and was a C→T transition at position 506 relative to the predicted translation start site (TSS). This caused a Pro→Leu substitution at position 169 of the encoded protein (Supplemental Figure 1). The gene At3g03990 is At-*D14* (Waters et al., 2012b), the ortholog of rice *D14* (Arite et al., 2009; Gao et al., 2009; Liu et al., 2009) and petunia *DAD2* (Hamiaux et al., 2012). These loci are required for SL-dependent inhibition of shoot branching.

The F1 progeny from crosses between *seto5* mutants and the strong mutant *d14-1* in which full-length transcripts are undetectable (Waters et al., 2012b; Supplemental Figure 2A) were phenotypically mutant: They showed an increased number of primary rosette branches and reduced stature relative to wild-type plants (Supplemental Figures 2B and 2C). This confirmed that the phenotype of *seto5* was caused by the point mutation in *D14*, and we renamed this mutant *d14-seto*. A 2.3-kb genomic region comprising 553 bp 5′ of the TSS, the 804-bp coding sequence (CDS), and a 916-bp region 3′of the stop codon (Supplemental Figure 2A) of *D14* was sufficient to complement the *d14-seto* mutation (Supplemental Figures 2D and 2E), indicating that this sequence contained the regulatory regions necessary for *D14* function. Constructs carrying only the 553 bp 5′ of the TSS and the 804-bp CDS also rescued the *d14-seto* mutant phenotype (Supplemental Figure 2F).

We analyzed the phenotype of two additional mutant lines with T-DNA insertions at 153 and 71 bp 5′ of the *D14* TSS, termed *d14-3* and *d14-4*, respectively (SALK_057876 and GABI-KAT-759C03; Supplemental Figure 2A). Neither showed excess of branching or reduced stature in the homozygous condition nor in heteroallelic combination with *d14-seto* (Supplemental Figure 2B) despite *d14-3* showing significantly reduced levels of *D14* mRNA (Supplemental Figure 3). This suggests that *D14* mRNA levels are not limiting in *Arabidopsis*. We also generated *d14-seto max2-1* double mutants whose phenotype resembled that of *max2-1* plants (Figures 1H and 1I), confirming *D14* involvement in the SL pathway.

In summary, the *d14-seto* mutant is a strong loss-of-function allele of *D14* that carries a point mutation in the CDS of the gene.

Relationship between *D14* and *BRC1*

It has been proposed that *BRC1* is downstream of the SL pathway in pea, *Arabidopsis*, and rice (Aguilar-Martínez et al., 2007; Finlayson, 2007; Brewer et al., 2009; Braun et al., 2012; Dun et al., 2012, 2013; Minakuchi et al., 2010). To further test this relationship, we studied transcript levels of each gene in cauline leaves and axillary buds of the reciprocal single mutant. *D14* mRNA levels were unaltered in *brc1-2* mutants (Figures 2A and 2B), whereas *BRC1* mRNA levels were greatly reduced in *d14-seto* mutants, in both axillary buds and cauline leaves (Figures 2A and 2B). Then, we studied the branching and height phenotypes of wild-type, *d14-seto*, and *brc1-2* plants as well as double mutant *d14-seto brc1-2* plants. Double mutants had significantly more branches than the single mutants, indicating additivity of the phenotypes (Figure 2C). This was in contrast with the flowering time and height phenotypes, which showed no additivity (Figures 1G and 2D).

These results support both the transcriptional regulation of *BRC1* by the SL pathway and also partially nonoverlapping roles for *BRC1* and SL-related genes in the regulation of shoot branching (see Discussion).

The d14-seto Protein

D14 belongs to the α/β-fold hydrolase superfamily (Ishikawa et al., 2005; Arite et al., 2009). The crystal structures of petunia DAD2, rice D14, *Arabidopsis* D14, and KAI2 show that they have a canonical α/β-fold hydrolase domain with a substrate binding pocket and the Ser-His-Asp catalytic triad necessary for hydrolase activity. A cap formed by four helices partially covers the active site with nonpolar residues (Hamiaux et al., 2012; Bythell-Douglas et al., 2013; Guo et al., 2013b; Kagiyama et al., 2013; Zhao et al., 2013; Figure 3C). In D14 proteins, the pocket can bind the synthetic SL analog GR24 (Hamiaux et al., 2012; Kagiyama et al., 2013; Nakamura et al., 2013). In KAI2, the pocket binds the synthetic KAR KAR$_1$ (Bythell-Douglas et al., 2013; Guo et al., 2013b; Kagiyama et al., 2013). Protein destabilization and conformational changes have been detected after ligand binding in both protein types (Hamiaux et al., 2012; Guo et al., 2013b; Nakamura et al., 2013).

The strong phenotype of *d14-seto*, which has a single Pro169Leu substitution, suggested an important role for this residue. We mapped this position in the 3D protein structure using PyMOL (www.pymol.org) and found that it is located at the N terminus of cap helix αD3, with the side chain exposed to the solvent (Figures 3A and 3C to 3E; Supplemental Figure 4). To study potential

Figure 1. (continued).

(C) Number of primary rosette branches (RI) of wild-type and *d14-seto* plants.

(D) Number of secondary branches (RII+CII) relative to the number of primary branches (RI+CI).

(E) Height of the main inflorescence of the same set of plants.

(F) Developmental stages of buds in the axils of cotyledons (C1 and C2) and rosette leaves (L1 to L10) of wild-type (top) and *d14-seto* (bottom) individuals. R, reproductive stage, V1 to V3, vegetative stages; LP, leaf primordium stages; M, meristem; E, empty axil. Developmental stages are as defined (Aguilar-Martínez et al., 2007) (n = 10).

(G) Flowering time, expressed as number of leaves, of lateral inflorescences of wild-type, *d14-seto*, and *brc1-2* mutants and *d14-seto brc1-2* double mutants. −1, uppermost RI; +1 and +2, first and second basal-most CI branches.

(H) and **(I)** Number of RI branches **(H)** and height of the main inflorescence **(I)** of *d14-seto max2-1* double mutants. Asterisks denote significant differences in Student's t tests ($P < 0.0001$). Letters denote significant differences in one-way ANOVA test (Tukey test $P < 0.05$). Data shown as mean ± SE (n = 20).

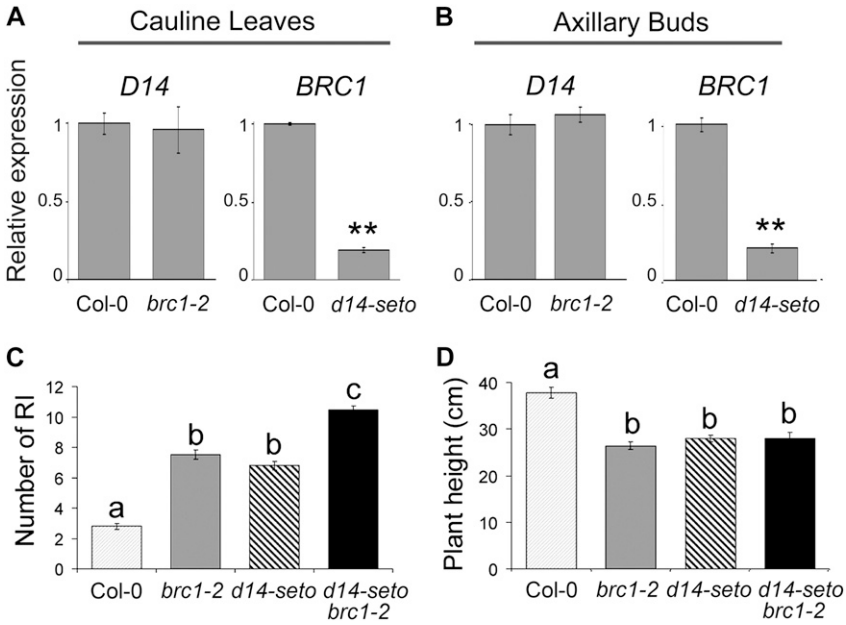

Figure 2. Genetic Relationship between *BRC1* and *D14*.

(A) and **(B)** Transcript abundance of *D14* and *BRC1* in cauline leaves **(A)** and axillary buds **(B)** of wild-type, *d14-seto*, and *brc1-2* quantified by qPCR. Data shown as mean ±SE (n = 3 to 5 biological replicates). Asterisks denote significant differences in Student's t test (**P < 0.01).

(C) Number of RI (primary rosette branches) of wild-type, *brc1-2*, *d14-seto*, and *d14-seto brc1-2* F3 plant siblings.

(D) Height of the main inflorescence of the same plants. Letters denote significant differences in one-way ANOVA test (Tukey test P < 0.05). Data shown as mean ±SE (n = 20).

destabilizing effects of this mutation, we compared the differences in free energy of unfolding (ΔΔG) between the wild-type and mutant proteins. No large destabilizing effects were predicted for this mutation (Supplemental Table 1).

Sequence comparison of a large collection of D14-related proteins revealed that Pro-169 is fully conserved among D14-related proteins, while KAI2-related proteins have a highly conserved Ser in this position (Figure 3A; Supplemental Figure 4). Indeed, Pro-169/Ser-168 is a specificity-determining position (SDP; de Juan et al., 2013) that may provide functional specificity to D14 and KAI2 (Figure 3B). This position is adjacent to a loop whose length and composition also differ between D14-type and KAI2-type proteins (Figures 3A, 3C, and 3D; Supplemental Figure 4).

KAR_1 binding to KAI2 causes conformational changes in the side chains of 11 KAI2 protein residues (Guo et al., 2013b). Four of them (Met-166, Ile-169, Glu-173, and Arg-176) are in close proximity to Ser-168 (Supplemental Figure 5). Mapping of the equivalent residues in D14 (Val-168, Ala-170, Glu-174, and Arg-177; Supplemental Figure 4) confirmed that they also cluster around Pro-169 (Figure 3E).

In summary, the *d14-seto* allele has a Pro→Leu mutation in an SDP located not in the active site, but in the external surface of one of the D14 protein cap helices. Calculations of free energy of unfolding (ΔΔG) indicate that this mutation should not destabilize the 3D structure. However, this mutation is located in a protein surface region that, by analogy with KAI2, could undergo conformational changes after SL binding and interfere with protein–protein interactions essential for functional SL signaling.

D14 Expression Patterns and Protein Distribution during *Arabidopsis* Development

To identify the plant tissues in which *D14* has an important role, we studied its mRNA and protein distribution during plant development. First, we analyzed its mRNA levels in different tissues by quantitative real-time PCR (qPCR). In 28-d-old plants grown in long days (which had undergone flowering), *D14* was transcribed at high levels in rosette and cauline leaves and at lower levels in axillary buds, inflorescences, stems, and roots (Supplemental Figure 6).

We then generated transcriptional and translational fusions lines of *D14*. For this, we made three constructs carrying the 540 bp upstream of the *D14* TSS fused to the CDS of the β-*GLUCURONIDASE* (*GUS*) gene (*D14pro:GUS*) or the same *D14* promoter region fused to the CDSs of *D14* and *GUS* or *GREEN FLUORESCENT PROTEIN* (*GFP*; *D14pro:D14:GUS* or *D14pro:D14:GFP*). These two types of lines could complement the phenotype of *d14-seto* mutants (Supplemental Figure 2). We studied *GUS*/*GFP* expression in nine representative T3 homozygous lines. In 5-d-old *D14pro:GUS* seedlings, *GUS* staining accumulated in the root and in the developing vascular tissue of cotyledons. Root expression became progressively restricted to the vascular cylinder (Figure 4A). In 10-d-old seedlings, the vascular tissue of the hypocotyl also showed *GUS* activity (Figure 4B). In general, root

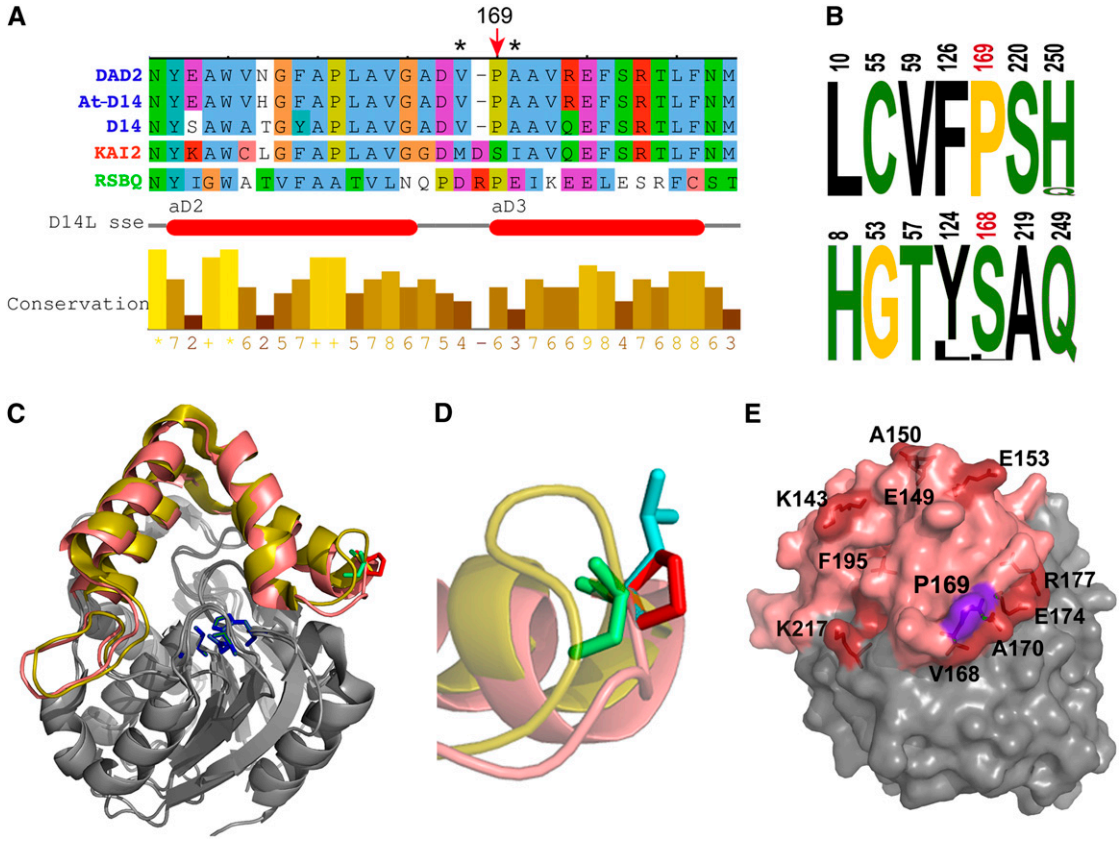

Figure 3. The d14-seto Protein.

(A) Sequence alignment of the *Arabidopsis* D14 segment comprising the Pro169Leu mutation, with ortholog sequences petunia DAD2 (Hamiaux et al., 2012), rice D14 (Arite et al., 2009; Gao et al., 2009; Liu et al., 2009; Hamiaux et al., 2012), paralog KAI2 (Waters et al., 2012b), and related bacterial protein RsbQ (Brody et al., 2001). Red arrow indicates Pro-169 and corresponding amino acid Ser-168 in KAI2. Asterisks indicate residues Met-166 and Ile-169, which undergo conformational changes in KAI2 after KAR_1 binding (Guo et al., 2013b). Horizontal red bars indicate the position of two of the KAI2 cap α-helices (Kagiyama et al., 2013).

(B) Logos of SDPs that differ in D14 (top) and KAI2 (bottom) ortholog sequences. Numbering corresponds to D14 and KAI2 protein sequences. Pro-169 and Ser-168 are shown in red. Hydrophobic residues are indicated in black, polar residues in green, and Gly and Pro in yellow. Letter size represents percentage of conservation within protein classes.

(C) Front view of D14 (PDB:4ih4) and KAI2 (PDB:3w06) structural alignment. Helical caps of D14 and KAI2 are highlighted in salmon pink and yellow, respectively. Active site residues are in blue, D14 Pro-169 is in red, and KAI2 S168 is in green.

(D) Close-up view and side chain superposition of wild-type D14 P169 (red), mutant Leu-169 (blue), and KAI2 Ser-168 (green). Note that the Pro-169 side chain is exposed to the solvent and that KAI2 loop (yellow) is longer than that of D14.

(E) D14 structure in surface representation. Residues corresponding to residues in KAI2 that undergo side-chain movement after KAR_1 binding are labeled and highlighted in red, Pro-169 in purple and cap domain in pink.

expression was undetectable in the meristematic zone but was strong in the differentiation zone and detectable in the elongation zone of some lines (Figure 4L). Analysis of thin sections of plastic-embedded roots confirmed that *GUS* expression was progressively restricted to phloem strands (Figures 4M to 4O). The lack of expression in the root meristem and GUS accumulation in root phloem cells was consistent with previous high-resolution expression profilings (Brady et al., 2007). In the aerial part, the *D14* promoter was active throughout leaf primordia and young leaves (Figures 4B and 4C). Expression was progressively restricted to the phloem in expanding cotyledons, leaves, sepals, petals, and stamen filaments (Figures 4B, 4D, 4I, and 4K) and was almost undetectable in mature leaves (Figure 4E). *GUS* signal was also strong in the style (Figure 4K), flower pedicels (Figure 4J), and the apical-most region of the inflorescence stems but not in the basal-most region (Figures 4F and 4J). Thin sections showed that GUS accumulated in a ring of cortex cells in the stem (Figures 4P and 4Q). Cortex sectors adjacent to the vascular bundles showed more *GUS* expression that those next to interfascicular regions (Figures 4P and 4Q). In addition, the *D14* promoter was active throughout axillary buds (Figures 4G and 4H). The general distribution of D14:GUS in *D14pro*:*D14*:*GUS* lines paralleled that of the promoter activity but D14:GUS was more widespread: In nine independent homozygous lines, the

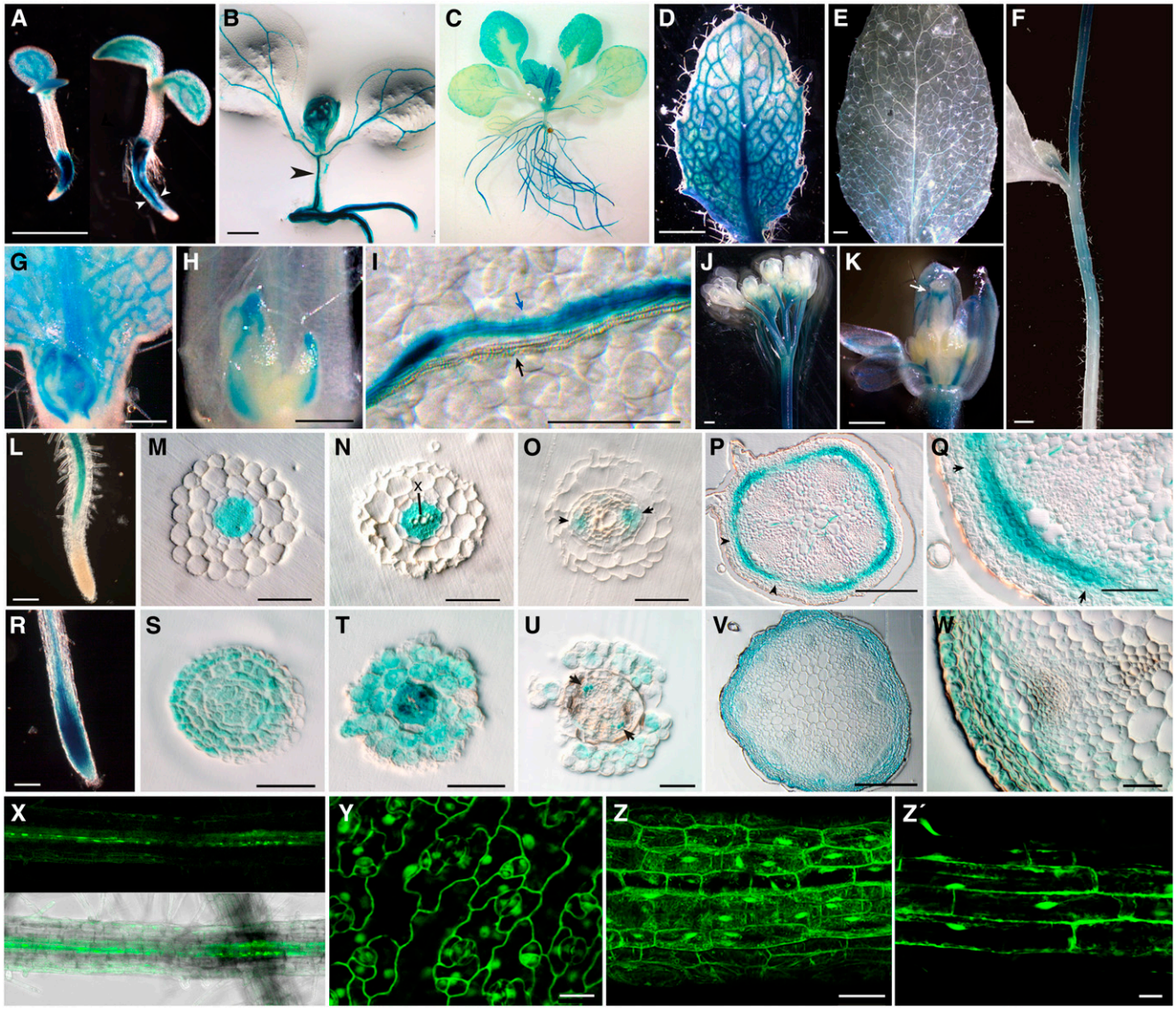

Figure 4. *D14* Promoter Activity and D14 Protein Distribution during *Arabidopsis* Development.

GUS histochemical activity of *Arabidopsis D14pro:GUS* (**[A]** to **[Q]**) and *D14pro:D14:GUS* (**[R]** to **[W]**) transgenic plants.
(A) Five-day-old transgenic seedlings. The plant on the right, more advanced in development, shows expression in the root more restricted to the vascular cylinder (arrowheads) than that of the less developmentally advanced (left).
(B) Ten-day-old seedling with *GUS* activity in the vascular tissue of the hypocotyl (arrowhead).
(C) Eighteen-day-old vegetative rosette.
(D) Young rosette leaf from plant in **(C)**.
(E) Mature cauline leaf from 30-day-old plant.
(F) Stem of the main inflorescence showing a gradient of *GUS* activity with a maximum near the apex.
(G) Bud in the axil of a young rosette leaf.
(H) Bud in the axil of a mature rosette leaf.
(I) Detail of a rosette leaf surface. Note the separation between the xylem (white) bundle (black arrow) and the phloem (blue) bundle expressing *GUS* (blue arrow).
(J) Main inflorescence. GUS accumulates in the apical-most stem region and in flower pedicels.
(K) Close-up of a developing flower. Signal in the style is indicated (white arrow).
(L) Root tip.
(M) to **(O)** The 3-μm transverse plastic-embedded sections of root similar to that in **(L)**.
(M) Distal section showing *GUS* staining in procambium cells.
(N) GUS is excluded from xylem cells (X).

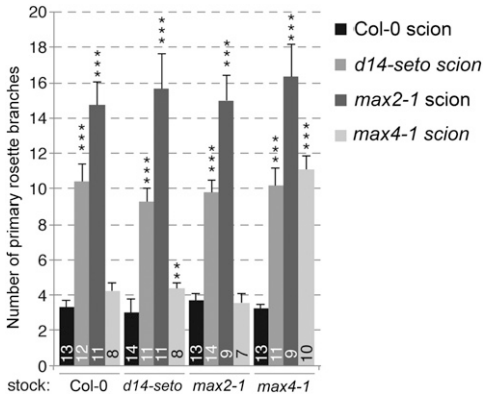

Figure 5. Spatial Requirement of *D14* to Suppress Branching.

Number of rosette branches in plants obtained from the micrografts indicated, quantified 14 d after bolting. Data shown as mean ± SE. Numbers on bars indicate the number of individuals analyzed. **P < 0.01; ***P < 0.001.

protein was also detected in the root meristem (Figures 4R and 4S), root and shoot epidermis (Figures 4T to 4W), and shoot vasculature (Figures 4U and 4W).

D14:GFP subcellular localization, analyzed in *D14pro:D14:GFP* and *CaMV35Spro:D14:GFP* lines, was both cytoplasmic and nuclear in all tissues studied (Figures 4X to 4Z), consistent with WoLF PSORT predictions (Horton et al., 2007).

D14 Does Not Move Long Distances Acropetally in the Plant to Regulate Shoot Branching

To test whether *D14* could act non-cell autonomously in the regulation of shoot branching, we performed reciprocal micrografting between wild-type, *d14-seto*, *max2-1*, and *max4-1* rootstocks and scions and studied their branching phenotypes (Figure 5). If the *D14* mRNA or protein moved long distance acropetally or if *D14* was exclusively involved in the synthesis of a bioactive compound transported upwards in the plant, *d14-seto* scions grafted to wild-type stocks would have a wild-type, or at least a partially rescued, branching phenotype. Instead, we found that *d14-seto* scions grafted to either wild-type, *max2-1*, or *max4-1* rootstocks remained bushy, like *max2-1* scions (Figure 5). This was in agreement with grafting experiments performed with *dad2* in petunia (Simons et al., 2007) and indicated that, like MAX2, D14 is required locally in the aerial part of the plant to suppress shoot branching. This is also consistent with the proposed interaction between D14 and MAX2 and with a role for *D14* in SL perception and signaling.

D14 Transcription Is Neither Responsive to SL nor Auxin Signaling nor to Bud Growth Status

To analyze *D14* transcriptional regulation, we tested whether expression of this gene was affected by SL or auxin signaling, as described for other SL-related genes (Sorefan et al., 2003; Bainbridge et al., 2005; Foo et al., 2005; Snowden et al., 2005; Johnson et al., 2006; Zou et al., 2006; Arite et al., 2007; Simons et al., 2007; Hayward et al., 2009; Mashiguchi et al., 2009; Guan et al., 2012; Waters et al., 2012b) or by bud growth status, like petunia *DAD2* (Hamiaux et al., 2012).

We quantified *D14* transcript levels in young seedlings, cauline leaves, and axillary buds of *max2-1*, *max4-1*, and *d14-seto* mutants. Expression of *D14* did not change significantly in any background or plant tissue, except for a slight reduction in transcript levels in *d14-seto* mutant axillary buds (Figure 6A). We then treated young wild-type seedlings with 5 μM synthetic SL GR24 (24 h), which confirmed that *D14* mRNA levels were unresponsive to GR24. *MAX2*, by contrast, responded negatively to GR24 (Figure 6B). To test whether *D14* transcription is positively regulated by auxin levels or transport, we compared *D14* mRNA levels of young seedlings treated with synthetic auxin 1-naphthaleneacetic acid (NAA), the auxin transport inhibitor 1-*N*-naphthylphthalamic acid (NPA), or the mock control (24 h). *D14* transcript levels showed only moderate reduction in NPA-treated plants (Figure 6C). In a second experiment, we monitored the response of the *D14* promoter to NAA or NPA treatment (24 h) in *D14pro:GUS* seedlings; there were no significant changes in *GUS* activity in treated relative to mock-treated seedlings (Figure 6F), although NAA effectively activated the synthetic auxin response promoter *DR5* (Figure 6G).

Finally, in axillary bud tissue, we studied the transcriptional response of *D14* to treatments affecting bud growth status,

Figure 4. (continued).

(O) More proximal section showing promoter activity in phloem cells (arrows).
(P) Transverse plastic-embedded section of a stem internode of the primary inflorescence.
(Q) Close-up of a section similar to that shown in **(M)**, with cortex cells but not epidermis cells expressing *GUS*. Notice the stronger signal in the vascular bundle sector flanked by the arrows in **(P)** and **(Q)**.
(R) Root tip similar to that in **(L)**. D14:GUS is present in the root tip.
(S) to **(U)** The 3-μm transverse plastic-embedded sections of root tips. **(S)** shows the meristematic zone, and **(T)** and **(U)** are sections similar to those in **(N)** and **(O)**. *GUS* signal is widespread in **(S)** and **(T)** and accumulates in the epidermis, cortex, and phloem (arrowheads) in **(U)**.
(V) and **(W)** Stem transverse plastic-embedded sections comparable to those in **(P)** to **(Q)**. GUS is detectable throughout the cortex, epidermis, and phloem (arrowheads).
(X) GFP fluorescence image (top) and fluorescence merged with bright-field image (bottom) of a transgenic *D14pro:D14:GFP* root.
(Y) to **(Z')** Leaf **(Y)**, hypocotyl **(Z)**, and root **(Z')** cells of *CaMV35Spro:D14:GFP* transgenic plants. GFP is detected in nucleus and cytoplasm.
Bars = 1 mm in **(A)**, **(D)** to **(F)**, and **(K)**, 500 μm in **(L)**, 200 μm in **(B)**, **(M)**, and **(P)**, 100 μm in **(G)** and **(N)**, 50 μm in **(H)** to **(J)**, **(Q)**, and **(Z)**, 15 μm in **(Y)** and **(Z')**.

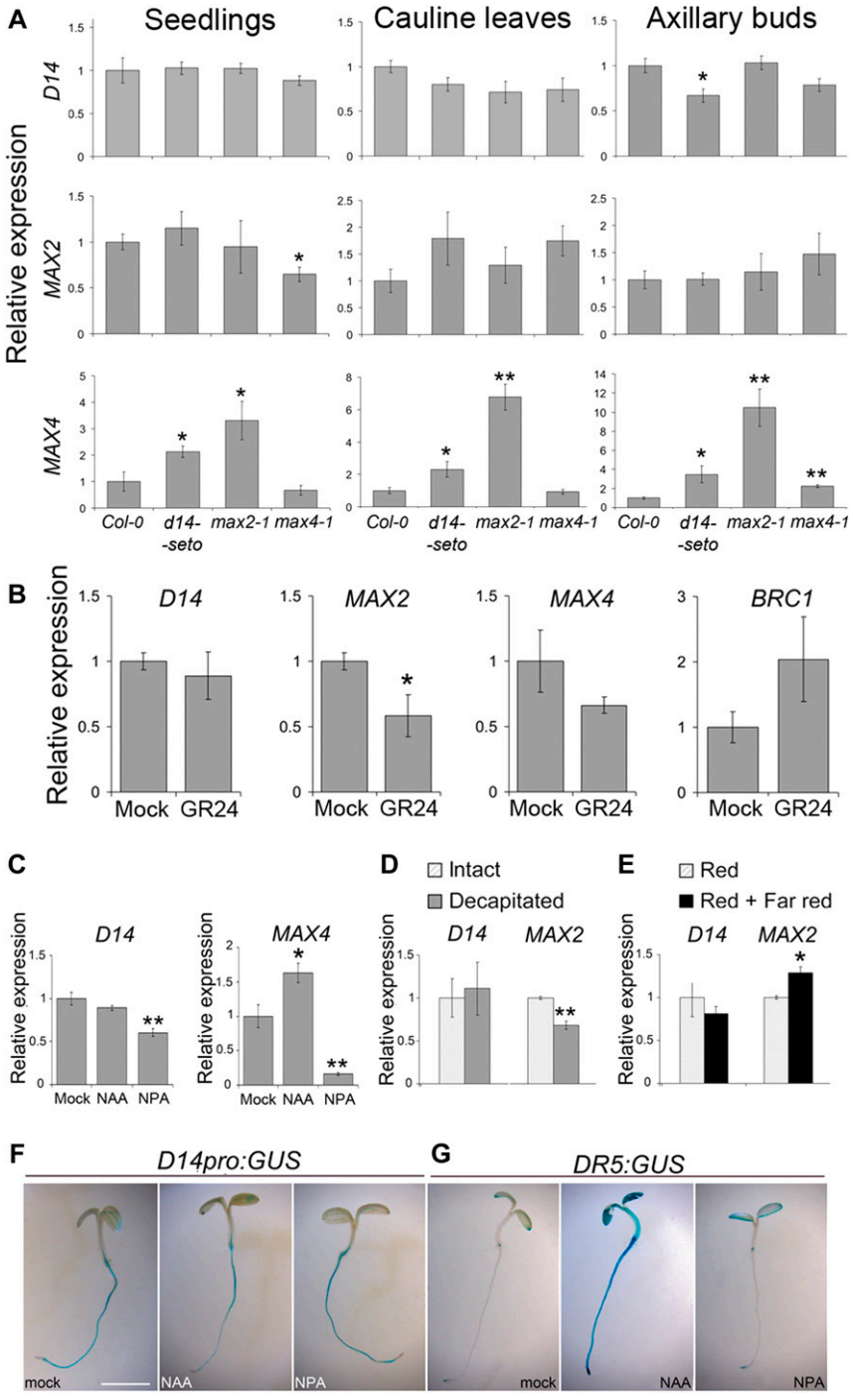

Figure 6. Transcriptional Regulation of *D14*.

(A) qPCR quantification of *D14*, *MAX2*, and *MAX4* transcript abundance in seedlings, cauline leaves, and axillary buds of *d14-seto*, *max2-1*, or *max4-1* plants relative to levels in wild-type Col-0 plants.

(B) Transcript abundance of *D14*, *MAX2*, and *MAX4* and *BRC1* in seedlings treated for 24 h with 5 μM GR24 (synthetic SL analog) compared with mock-treated plants.

(C) *D14* and *MAX4* transcript levels in 10-d-old seedlings treated with 10 μM NAA or 10 μM NPA (auxin transport inhibitor) relative to levels in mock-treated plants.

(D) and **(E)** *D14* and *MAX2* mRNA levels measured in axillary buds of decapitated plants 8 h after treatment relative to levels in intact plants grown in parallel **(D)** and of plants treated with red + far-red light for 8 h relative to levels in red light–treated plants grown in parallel **(E)**.

including decapitation of the main shoot, which promotes bud activation, and 8-h exposure to far-red-rich light, which promotes bud dormancy. *D14* mRNA levels were unaffected by both treatments (Figures 6D and 6E), whereas *MAX2* mRNA levels correlated positively with bud dormancy in both cases (Figures 6D and 6E).

These results show that *D14* mRNA levels are thus not responsive to changes in SL or auxin signaling, nor do they correlate positively with bud growth arrest in *Arabidopsis*.

The D14 Protein Is Rapidly Degraded in the Presence of SL

As *D14* did not appear to be regulated transcriptionally, we investigated a potential posttranslational regulation. To test whether the D14 protein was regulated by SL, we treated young seedlings carrying either *D14pro:D14:GUS/GFP* or *CaMV35Spro:D14:GFP* constructs with GR24 and studied D14:GUS and D14:GFP protein levels at different times. When incubated for 24 h with 5 μM GR24, plants showed a striking reduction in GUS and GFP signal especially in rosette leaves and hypocotyl, although the effect was also noticeable in roots (Figures 7A and 7C to 7G; Supplemental Figure 7). By contrast, *max2-1* mutant plants carrying the same constructs did not show reduced levels of GUS/GFP when treated with GR24 (Figures 7B and 7G; Supplemental Figure 8). GR24-treated *D14pro:GUS* control plants did not display reduced GUS protein levels (Supplemental Figure 9).

We then performed a time-course analysis of the response in *Arabidopsis*. We did immunoblots with α-GFP in *D14pro:D14:GFP* seedlings treated 1, 2, 4, 6, 8, and 24 h with 5 μM GR24 and detected a negative effect of GR24 on D14:GFP accumulation as early as 1 to 2 h after the beginning of the GR24 treatment (Figure 7H). Protein levels begun to recover 26 h later, even in the presence of GR24, perhaps due to GR24 hydrolysis by D14 and new protein synthesis. Removal of GR24 after 24 h led to accelerated protein accumulation (Figure 7I). The effect of GR24 was dose dependent and still detectable at GR24 concentrations of 50 to 100 nM (Figure 7J). This response was strongly suppressed by simultaneous treatment of plants with the proteasome inhibitor MG132 (Figure 7K).

All these results indicate that SL promotes rapid degradation of D14 and that this response requires a functional *MAX2* gene. If D14 is the SL receptor, as proposed, this negative feedback regulation would cause a substantial drop in SL perception that could very effectively limit the extent of SL signaling.

DISCUSSION

D14 as an SL Receptor

Two alternative roles have been proposed for D14-type proteins in plants, as enzymes that transform SL into bioactive compounds and as SL receptors. Growing evidence supports the latter possibility and suggests that D14 links SL perception and signaling through protein–protein interactions with MAX2-type proteins (Arite et al., 2009; Hamiaux et al., 2012; Waters et al., 2012b; Kagiyama et al., 2013). Our grafting experiments, which show that the bushy phenotype of *d14-seto* mutants cannot be rescued by grafting their shoots to wild-type rootstocks, are consistent with grafting experiments performed with *dad2-1* in petunia (Simons et al., 2007) and confirm a local requirement for D14 in the aerial part of the plant. This is in agreement with the proposal that D14 and MAX2 (also required in the shoot for branch suppression; Booker et al., 2005; Stirnberg et al., 2007) must interact to trigger SL signaling.

Spatial Regulation of SL Signaling

According to the recent model, D14 and MAX2 interact in the presence of SL (Hamiaux et al., 2012; Zhou et al., 2013; Jiang et al., 2013), although in *Arabidopsis*, this interaction may not be direct (Wang et al., 2013). As MAX2, D14, and SL are not distributed ubiquitously, the SL response would only take place in tissues in which these three factors coincide. MAX2 is widely distributed in axillary buds, young leaves, hypocotyl, vasculature, and flower organs (Shen et al., 2007; Stirnberg et al., 2007). *D14* expression patterns and protein distribution largely overlap with those of MAX2 in axillary buds, root vasculature, and carpel. Moreover, the wider distribution of GUS in *D14pro:D14:GUS* relative to *D14pro:GUS* lines raises the possibility that the D14 protein moves, at least within a short range, and is perhaps unloaded from the root phloem. Alternatively, regulatory motifs within the open reading frame of *D14* could, in *D14pro:D14:GUS* lines, regulate transcription in tissues adjacent to those identified using the *D14pro:GUS* lines. In situ hybridization of *D14* mRNA and immunolocalization of the D14 protein will help elucidate these possibilities. In some other tissues, such as the shoot cambium, where *MAX2* has been shown to play an essential role (Agusti and Greb, 2013), the D14 protein does not accumulate measurably. One possibility is that MAX2 does not interact with D14 for this function; alternatively, small, below-detection amounts of D14, which perhaps is degraded rapidly after the interaction, are sufficient to trigger SL signaling in this tissue. At the subcellular level, the nuclear localization of MAX2 (Shen et al., 2007; Stirnberg et al., 2007) and D14 (which is nuclear and cytoplasmic) would allow their physical interactions in the nucleus without special translocation events.

By contrast, the interaction between SL and D14 may need to be promoted. SL has been shown to be transported in the xylem sap (Foo et al., 2001; Kohlen et al., 2011) where D14 is undetectable. Moreover, some *D14*- and *MAX2*-expressing tissues, such as very young axillary buds, whose development responds to SL signaling, are not yet connected to the vasculature. Although SL accumulation in phloem and other tissues is

Figure 6. (continued).

(F) and **(G)** Histochemical assays of *D14pro:GUS* **(F)** and *DR5:GUS* **(G)** in 4-d-old seedlings treated for 24 h with 10 μM NAA, 10 μM NPA, or mock. Bar = 1 mm for **(F)** and **(G)**. Data shown as mean ± SE (n = 3 to 4 biological replicates). Asterisks denote significant differences in Student's t test (*P < 0.05; **P < 0.01).

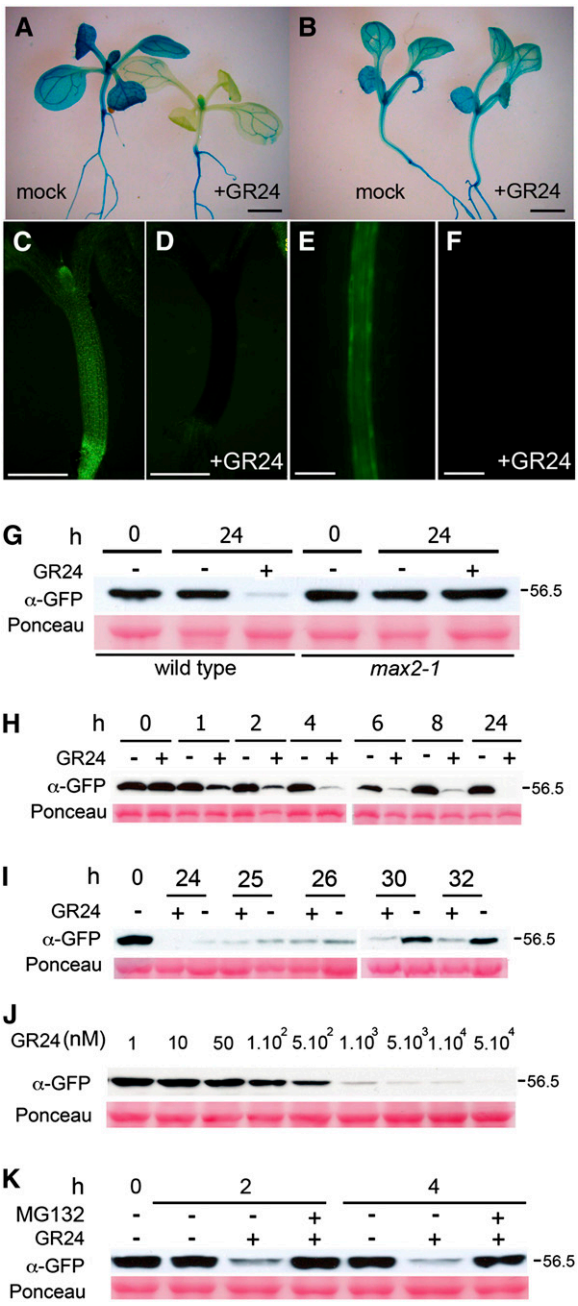

Figure 7. SL Destabilizes the D14 Protein.

(A) to **(F)** *GUS* histochemical activity of *D14pro:D14:GUS* plants in Col-0 **(A)** or *max2-1* **(B)** background after 24-h treatment with mock (left) or GR24 (right). Fluorescence image of young *CaMV35Spro:D14:GFP* seedlings after 24-h treatment with mock **(C)** or GR24 **(D)**. Fluorescence image of *D14pro:D14:GFP* seedlings after 24-h treatment with mock **(E)** or GR24 **(F)**. Bars = 500 μm.

(G) D14:GFP response to GR24 analyzed by immunoblot using α-GFP antibody in *D14pro:D14:GUS* plants in Col-0 (wild type) or *max2-1*.

(H) Time course of D14:GFP accumulation in response to GR24. Protein extracts (10 μg) from 5-d-old *D14pro:D14:GFP* seedlings treated with GR24 (+) or mock (−) for 0 to 24 h were separated by 10% SDS-PAGE and identified as a 56.5-kD band.

(I) After a 24-h GR24 treatment, seedlings were maintained in MS with (+) or without GR24 (−) for 1 to 8 h.

(J) Dose response of D14:GFP to 24-h treatments with increasingly higher concentrations of GR24.

(K) D14:GFP response to GR24 in the presence of MG132. In **(G)** to **(K)**, Ponceau stainings are included for loading reference. All GR24 treatments used a 5 μM concentration unless indicated.

yet unknown, this seems to imply that a system of cell-to-cell SL delivery may be required to regulate SL–D14 interactions. Such a system has been described in petunia, where it is regulated by the ABC transporter PDR1 (Kretzschmar et al., 2012). *Arabidopsis* SL transporters have not yet been identified, but transgenic plants carrying the *PDR1pro:GUS* construct show promoter activity in the vascular tissue, stem nodes, and regions that subtend axillary buds (Kretzschmar et al., 2012). SL might be exported from the xylem to the basal region of buds, thus promoting bud arrest.

The d14-seto Protein

We identified *d14-seto*, a loss-of-function mutant allele in the *D14* locus, which has a single Pro169Leu amino acid substitution and causes a consistently strong, bushy phenotype. The Pro-169 position is probably not involved in ligand binding or hydrolytic activity, nor is the Pro169Leu mutation predicted to cause large destabilizing effects in the protein structure. Pro-169 is located in the external surface of the cap domain with the side chain exposed to the solvent, suggesting that the mutation affects critical protein–protein interactions. This position is one of the seven SDPs (Rausell et al., 2010) found between D14 and KAI2 proteins, which have either conserved Pro or Ser, respectively, suggesting that these residues help determine the functional specificity of each protein type. It is also unlikely that they are involved in D14–MAX2 interactions, as both D14 and KAI2 seem to interact with MAX2, based on molecular and genetic evidence (Nelson et al., 2011; Hamiaux et al., 2012; Waters et al., 2012b; Kagiyama et al., 2013).

Pro-169 could participate in the recognition of sets of proteins to be targeted for degradation through the SL pathway, such as D53-, BES1-, or DELLA-related proteins (Jiang et al., 2013; Nakamura et al., 2013; Wang et al., 2013; Zhou et al., 2013). The equivalent position in KAI2, Ser-168, is surrounded by amino acids that undergo measurable conformational changes upon KAR_1-KAI2 binding (Guo et al., 2013b). If this situation is analogous for D14, SL binding and/or hydrolysis could cause allosteric changes in the area surrounding Pro-169, creating or modifying a protein-interacting surface. This model would resemble that of the gibberellin receptor GID1, an α/β-fold hydrolase superfamily protein, in which gibberellin acts as an allosteric effector and induces conformational changes in the cap that folds back to generate a DELLA binding surface (Murase et al., 2008; Shimada et al., 2008). Further experiments will help evaluate this model; second-site mutagenesis and search for *d14-seto* suppressors could reveal additional components of the pathway acting in close proximity to the SL-D14 complex.

Relation of BRC1 and the SL Pathway

A positive transcriptional regulation of *BRC1* by the SL pathway has been proposed based on the strong downregulation of

BRC1 in axillary buds of SL mutants and its upregulation in buds in response to SL application (Aguilar-Martínez et al., 2007; Finlayson, 2007; Braun et al., 2012; Dun et al., 2012, 2013). However, these transcriptional changes could simply reflect SL-dependent bud dormancy or activity, to which *BRC1* expression is tightly associated. Now, we have also observed a strong transcriptional downregulation of *BRC1* in *d14-seto* cauline leaves, organs in which no obvious phenotypic effects are detected in *brc1* mutants. This supports a direct transcriptional regulation of *BRC1* by the SL pathway in organs different from axillary buds. Moreover, the late flowering phenotype of *d14-seto brc1-2* double mutants, identical to that of *brc1-2* mutants, suggests that in the control of flowering time, SLs could act entirely through regulation of *BRC1*, whose protein could in turn interact with FT, as described by Niwa et al. (2013). By contrast, the additive shoot branching phenotypes of *d14-seto* and *brc1-2* supports that SLs act not only by upregulating *BRC1* but also by other mechanisms not directly related to *BRC1* (i.e., PATS dampening and degradation of branching-promoting factors, such as D53 and BES1; Jiang et al., 2013; Wang et al., 2013; Zhou et al., 2013).

Conservation and Evolution of D14-Like Gene Regulation

Mutants bearing loss-of-function alleles of *D14*-like genes in rice (Arite et al., 2009; Gao et al., 2009; Liu et al., 2009), petunia (Hamiaux et al., 2012), and *Arabidopsis* (Waters et al., 2012b; this study) show increased branching and reduced stature, indicating functional conservation of these genes in the determination of plant architecture. Some degree of divergence in their regulation is nonetheless evident. For instance, the rice *D14* gene was reported to be transcribed in parenchyma cells surrounding the xylem (Arite et al., 2009), whereas in *Arabidopsis*, we found the strongest transcriptional activity of *D14* in the phloem, young organs, and cortex cells of elongating stems. Petunia *DAD2* and rice *D14* mRNA levels correlate positively with bud dormancy (Arite et al., 2009; Hamiaux et al., 2012), while this is not the case for *Arabidopsis D14*. In rice, *TB1* was proposed to be a transcriptional activator of *D14*. In protoplast assays, TB1 interacts with MADS57, a transcriptional repressor of *D14*, thus reducing the inhibitory effect on *D14* transcription (Guo et al., 2013a). If this regulatory pathway was conserved in *Arabidopsis*, we would predict that mutants in the Os-*Tb1* homolog, *BRC1*, would have reduced *D14* mRNA levels. We have found that this is not the case. Indeed, *D14* transcription levels are not greatly altered by any stimulus studied so far, with the exception of darkness (Waters and Smith, 2013). Effective regulation of protein stability in this group might have rendered its transcriptional regulation irrelevant, leading to evolutionary loss.

Negative Feedback Loops in SL Signaling

We observed that SL destabilizes D14, probably by promoting its proteasome-mediated degradation. If D14 is confirmed as the SL receptor, this would represent an example of an interesting phenomenon whereby a plant hormone triggers degradation of its own receptor. This response requires a functional *MAX2* gene, as we found that D14 is resistant to SL in *max2-1* mutants. MAX2 could participate directly in the SCF complex that tags D14 for degradation, implying that D14 could be a MAX2 substrate, like SLR1, D53, and BES1 (Jiang et al., 2013; Nakamura et al., 2013; Wang et al., 2013; Zhou et al., 2013). Alternatively, other proteins targeted by the SCF^{MAX2} complex might prevent D14 degradation, so that their removal during SL signal transduction could lead to D14 destabilization through other ubiquitin-related systems. Interestingly, while D53 and BES1 degradation occurs within 8 to 30 min after SL treatment, D14 degradation is slower, 1 to 2 h after SL treatment. This is in agreement with Jiang et al. (2013) and Zhou et al. (2013), who did not find SL-mediated destabilization of D14 in 1 h. One possible scenario is that once the SL-dependent substrates are degraded via the SL:D14:SCF^{MAX2} complex, D14 itself becomes destabilized. This negative feedback regulation to modulate D14 protein levels would cause a drop in SL perception that could effectively limit the extent of SL signaling. This scenario resembles that of the clock-associated protein EARLY FLOWERING3 that, after acting as substrate adaptor to promote recognition of GIGANTEA by the E3-ubiquitin ligase CONSTITUTIVE PHOTOMORPHOGENIC1 (COP1), is in turn ubiquitinated and degraded via COP1, leading to a cycling signaling (Yu et al., 2008).

In summary, SL signaling homeostasis seems to be modulated by a strong negative feedback regulation that affects not only the transcription of SL synthesis genes (Bainbridge et al., 2005; Foo et al., 2005; Snowden et al., 2005; Johnson et al., 2006; Arite et al., 2007; Drummond et al., 2009; Dun et al., 2009; Hayward et al., 2009) but also the stability of the D14 protein. The transcriptional regulatory mechanisms require functional SL signaling. This posttranslational regulation of D14 requires at least functional *MAX2*, but it remains unknown whether SL signal transduction is necessary. Assays performed using the d14-seto protein will help clarify this point.

Additional mechanisms that regulate this pathway might involve regulation of D14 cell-to-cell movement, modulation of SL transport, and/or availability and regulation of D14 nuclear localization to modulate the intensity of D14-MAX2 interactions. Further work is still needed to understand the stoichiometry of this process and the regulatory bottlenecks through which the signaling pathway is mostly regulated.

METHODS

Plant Material and Growth Conditions

Wild-type *Arabidopsis thaliana* was the Col-0 ecotype. The *d14-seto* allele was an ethyl methanesulfonate mutant generated by Lehle Seeds (www.arabidopsis.com). Homozygote seeds from plants backcrossed twice to wild type Col-0 were used. *d14-1* (NASC ID: N913109), *d14-3* (NASC ID: N678534), and *d14-4* (NASC ID: N557876) were obtained from the Nottingham Arabidopsis Stock Centre. *brc1-2* has been described (Aguilar-Martínez et al., 2007). *max2-1* and *max4-1* mutants were provided by O. Leyser. Wild-type and mutant seeds were sown on commercial soil and vermiculite at a 3:1 proportion, stratified in darkness (4°C, 3 d), and grown in a 16-h-light/8-h-dark photoperiod at 22°C in white light (W; PAR, 100 μmol m^{-2} s^{-1}). For the experiment in Figure 2D, seeds were grown in conditions as above and exposed for 8 h to white light (W; red [R]: far red [FR] ratio = 11.7) or W supplemented with FR (W+FR, R:FR ratio = 0.2) as described (González-Grandío et al., 2013). For auxin response assays, seedlings were germinated in vertical plates in Murashige and Skoog (MS) medium, 0.7% agar, 1% Suc (MAS) and grown as above for 15 d and then transferred to MAS + 10 μm NAA or MAS + mock (24 h).

Light Sources

White light was provided by cool-white 20-W F20T12/CW tubes (Phillips). Supplemental far-red light was provided by lamp tubes carrying far-red 735-nm LEDs (L735-03AU; EPITEX).

Protein Structure Analyses

Homolog sequences for D14, KAI2, and RsbQ were obtained by BLAST searches against the UniProt database. Sequence hits were further aligned with MUSCLE (Edgar, 2004). SDPs were analyzed with JDet (Muth et al., 2012) using the S3det method (Rausell et al., 2010) implemented in the JDet software. D14 (PDB:4ih4) and KAI2 (PDB:3w06) structures were aligned with FATCAT (Ye and Godzik, 2004). Mutant side chain orientation (Figure 3) was generated using FoldX (Schymkowitz et al., 2005). We identified residues of D14 corresponding to those in KAI2 undergoing side-chain movement after KAR_1 binding (Guo et al., 2013b). These residues were mapped in D14 structure (PDB:4ih4) using PyMOL (www.pymol.org). To assess the change in protein stability after mutation ($\Delta\Delta G$), we used the D14 structure (PDB:4ih4) with the prediction methods FoldX (Schymkowitz et al., 2005), I-Mutant (Capriotti et al., 2005), SDM (Worth et al., 2011), Eris (Yin et al., 2007), and Concoord/PBSA (Benedix et al., 2009).

Micrografting

Grafting was performed in tissue culture by joining shoot scions and root stocks of young, 6-d-old seedlings (grown on plates at 25°C in 16-h light days) at the level of their hypocotyls as described (Ragni et al., 2011). Successful grafts were transferred onto soil 7 d after grafting and grown in 16-h-light days. Phenotypes were scored 14 d after bolting.

Decapitation Assay

Col-0 plants were grown until main inflorescences were 2 to 3 cm in length. In half of the plants, the main shoot, including the cauline nodes, was removed; six to eight decapitated and nondecapitated rosettes were collected for each biological replicate 24 h after decapitation. RNA was extracted as described in González-Grandío et al. (2013), and qPCR was performed with three biological replicates.

Positional Cloning

The *seto5* mutation was mapped by the Instituto de Bioingeniería–Universidad Miguel Hernández Gene Mapping Facility (Elche, Spain) as described (Ponce et al., 1999, 2006). In brief, for low-resolution mapping, the DNA of 50 F2 phenotypically mutant plants was extracted individually and used as a template to multiplex PCR coamplify 32 SSLP and insertion/deletion molecular markers using fluorescently labeled oligonucleotides as primers. For fine mapping, 400 additional F2 plants were used to assess linkage iteratively between *seto5* and molecular markers designed according to the polymorphisms between Landsberg *erecta* and Col-0 described at the Monsanto Arabidopsis Polymorphism Collection database (http://www.arabidopsis.org).

Genome Sequencing

Whole-genome sequencing of 40 μg of pooled genomic DNA from six *seto5* individuals was performed by BGI (www.genomics.cn); 2.79 Gb of clean data was analyzed with an average effective depth of 22.75 X.

Phenotypic Analysis

Branches (shoots >1 cm) were counted 2 weeks after the main inflorescence became visible. AM initiation and early bud development phenotype analyses were performed as described (Aguilar-Martínez et al., 2007). Flowering time of cauline and rosette branches was analyzed by counting the number of rosette and cauline leaves.

Plastic Embedding of Stem Sections

Stem fragments (5 to 10 mm) from immediately above the uppermost rosette leaf were fixed in 4% glutaraldehyde and 0.1% Tween (20 to 24 h), dehydrated in ethanol series up to 100% ethanol, washed in preinfiltration solution (50% ethanol and 50% infiltration solution), and passed to the infiltration solution of the Historesin Standard kit (Leica). Subsequent steps were done according to the manufacturer's instructions. Sections (3 μm) of resin-embedded specimens were prepared with a Leica microtome and tungsten carbide blades, floated in a 50°C water bath, collected on a slide, and allowed to dry. Nontransgenic lines were stained with 1% cresyl violet (Sigma-Aldrich C-5042). Sections were mounted in Surgipath micromount (Leica).

GUS Histochemistry

GUS staining was performed as described (Sessions et al., 1999).

GR24 Treatments

Seedlings were grown in vertical MS + agar plates and were then transferred to liquid MS + 1% Suc medium with 5 μM GR24 (from a stock solution in acetone) or the corresponding acetone volume (mock) and grown in normal growth conditions for different times. When specified, other concentrations of GR24 were used. For the MG132 treatment, MG132 was added to a concentration of 50 μM at T0, and identical amounts were added to the incubation solution every hour. For the immunoblot experiments, 1-week-old seedlings were used.

Protein Extraction and Immunoblots

Five-day-old seedlings were frozen in liquid N_2, and total protein was extracted in PBS buffer, 0.1% SDS, 0.1% Triton X-100, 1 mM PMSF, 5 mM β-mercaptoethanol, and protease inhibitors (5 μM E-64, 50 μM leupeptin, 1 μM pepstatin, and 10 μg/mL aprotinin). The extract was centrifuged (15 min, 16,000*g*, 4°C), and the supernatant was collected. Protein concentration was determined in a Bradford assay. Protein extracts (10 μg) were denatured by boiling (5 min, 95°C), separated by 10% SDS-PAGE, and transferred to polyvinylidene difluoride membranes (Bio-Rad). To confirm equivalent protein loading, membranes were stained with Ponceau reagent. Membranes were probed with anti-GFP-horseradish peroxidase antibody (1:1000; Milteny Biotec), and signal was detected using ECL reagent (Invitrogen).

D14 Constructs

The CDS of *D14* and *d14-seto* and the 2.3-kb genomic fragment of *D14* and the *D14* promoter were amplified from genomic DNA using Phusion polymerase (Finnzymes) with indicated primers (Supplemental Table 2). The CDS of *MAX2* was amplified using indicated primers (Supplemental Table 2). PCR fragments were BP cloned into the entry vector pDONR207 (Gateway; Invitrogen). For the *CaMV35Spro:D14:GFP* construct, the CDS was LR cloned into the destination vector pGWB5. For *D14pro:GFP:D14*, the genomic fragment was cloned into pGWB4. For *D14pro:GUS*, the promoter was cloned into pGWB3. All pGW vectors were provided by Tsuyoshi Nakagawa (Shimane University; Nakagawa et al., 2007).

Arabidopsis Transgenic Plants

Transgenic plants (Col-0) were generated by agroinfiltration using the floral dip method (Clough and Bent, 1998). T3 homozygous lines

generated from T1 individuals carrying a single transgene insertion were analyzed.

RNA Preparation and qPCR Analyses

Material was harvested from at least eight individuals and a minimum of three biological replicates per genotype/treatment and stored in liquid N_2. RNA was isolated with the RNeasy plant mini kit (Qiagen). Possible traces of DNA were eliminated with an RNase-Free DNase set (Qiagen). RNA was used to make cDNA with the High-Capacity cDNA archive kit (Applied Biosystems). The qPCR reactions were performed with Power SYBR Green (Applied Biosystems) and the Applied Biosystems 7300 real-time PCR system, according to the manufacturer's instructions. Three technical replicates were done for each biological replicate. Primers pairs are described in Supplemental Table 2. The *SAND* gene was used as reference (Czechowski et al., 2005).

Accession Numbers

Sequence data from this article can be found in the GenBank/EMBL libraries under the following accession numbers: D14 (At3g03990), NM_111270.2; GI:30679007.

Supplemental Data

The following materials are available in the online version of this article.

Supplemental Figure 1. Mapping and Cloning of the *seto5* Locus.

Supplemental Figure 2. Complementation of the *d14-seto* Mutant and *D14* Allelic Series.

Supplemental Figure 3. Relative *D14* and *BRC1* mRNA Levels in Axillary Buds of the *d14-3* Mutant, Quantified by qPCR.

Supplemental Figure 4. Multiple Sequence Alignment of the D14 and KAI2 Orthologs.

Supplemental Figure 5. 3D Structure of D14 and KAI2 and Residues Affected upon KAR_1 Binding.

Supplemental Figure 6. *D14* Relative mRNA Levels in Different Tissues Analyzed by qPCR.

Supplemental Figure 7. The D14:GUS Protein Is Destabilized by SL.

Supplemental Figure 8. D14:GUS Is Not Destabilized by SL in a *max2-1* Background.

Supplemental Figure 9. GUS Is Not Destabilized by SL.

Supplemental Table 1. Difference in Free Energy of Unfolding between the Wild-Type D14 Protein and Mutant d14-seto Protein.

Supplemental Table 2. Primers Used in This Study.

ACKNOWLEDGMENTS

We thank Desmond Bradley, Eduardo González, and Michael Nicolas for helpful comments on the article, María Rosa Ponce, José Luis Micol, and the TRANSPLANTA Consortium for mapping the *seto5* mutant, Concepción Manzano for help with the mutant screening, Catherine Rameau and Binne Zwanenburg for GR24, Ottoline Leyser for seed stocks, Chidi Afamefule for qPCR of the *d14-3* mutants, and Catherine Mark for editorial assistance. This work was supported by the Spanish Ministerio de Educación y Ciencia (BIO2008-00581 and CSD2007-00057), Ministerio de Ciencia y Tecnología (BIO2011-25687), and the Fundación Ramón Areces.

AUTHOR CONTRIBUTIONS

F.C. and P.C. designed the research. F.C., K.N., C.S.H., M.L.R., J.C.S.-F., M.C., and P.C. performed the experiments. P.C., C.S.H., M.C., and F.C. analyzed the data. M.C. and J.C.S.-F. contributed analytical tools. P.C. wrote the article.

Received January 16, 2014; revised February 5, 2014; accepted February 11, 2014; published March 7, 2014.

REFERENCES

Aguilar-Martínez, J.A., Poza-Carrión, C., and Cubas, P. (2007). *Arabidopsis* BRANCHED1 acts as an integrator of branching signals within axillary buds. Plant Cell **19:** 458–472.

Agusti, J., and Greb, T. (2013). Going with the wind—Adaptive dynamics of plant secondary meristems. Mech. Dev. **130:** 34–44.

Alder, A., Jamil, M., Marzorati, M., Bruno, M., Vermathen, M., Bigler, P., Ghisla, S., Bouwmeester, H., Beyer, P., and Al-Babili, S. (2012). The path from β-carotene to carlactone, a strigolactone-like plant hormone. Science **335:** 1348–1351.

Arite, T., Iwata, H., Ohshima, K., Maekawa, M., Nakajima, M., Kojima, M., Sakakibara, H., and Kyozuka, J. (2007). DWARF10, an RMS1/MAX4/DAD1 ortholog, controls lateral bud outgrowth in rice. Plant J. **51:** 1019–1029.

Arite, T., Umehara, M., Ishikawa, S., Hanada, A., Maekawa, M., Yamaguchi, S., and Kyozuka, J. (2009). d14, a strigolactone-insensitive mutant of rice, shows an accelerated outgrowth of tillers. Plant Cell Physiol. **50:** 1416–1424.

Bainbridge, K., Sorefan, K., Ward, S., and Leyser, O. (2005). Hormonally controlled expression of the Arabidopsis MAX4 shoot branching regulatory gene. Plant J. **44:** 569–580.

Balla, J., Kalousek, P., Reinöhl, V., Friml, J., and Procházka, S. (2011). Competitive canalization of PIN-dependent auxin flow from axillary buds controls pea bud outgrowth. Plant J. **65:** 571–577.

Benedix, A., Becker, C.M., de Groot, B.L., Caflisch, A., and Böckmann, R.A. (2009). Predicting free energy changes using structural ensembles. Nat. Methods **6:** 3–4.

Bennett, T., Sieberer, T., Willett, B., Booker, J., Luschnig, C., and Leyser, O. (2006). The Arabidopsis MAX pathway controls shoot branching by regulating auxin transport. Curr. Biol. **16:** 553–563.

Booker, J., Sieberer, T., Wright, W., Williamson, L., Willett, B., Stirnberg, P., Turnbull, C., Srinivasan, M., Goddard, P., and Leyser, O. (2005). MAX1 encodes a cytochrome P450 family member that acts downstream of MAX3/4 to produce a carotenoid-derived branch-inhibiting hormone. Dev. Cell **8:** 443–449.

Brady, S.M., Orlando, D.A., Lee, J.Y., Wang, J.Y., Koch, J., Dinneny, J.R., Mace, D., Ohler, U., and Benfey, P.N. (2007). A high-resolution root spatiotemporal map reveals dominant expression patterns. Science **318:** 801–806.

Braun, N., et al. (2012). The pea TCP transcription factor PsBRC1 acts downstream of strigolactones to control shoot branching. Plant Physiol. **158:** 225–238.

Brewer, P.B., Dun, E.A., Ferguson, B.J., Rameau, C., and Beveridge, C.A. (2009). Strigolactone acts downstream of auxin to regulate bud outgrowth in pea and Arabidopsis. Plant Physiol. **150:** 482–493.

Brody, M.S., Vijay, K., and Price, C.W. (2001). Catalytic function of an alpha/beta hydrolase is required for energy stress activation of the sigma(B) transcription factor in *Bacillus subtilis*. J. Bacteriol. **183:** 6422–6428.

Bythell-Douglas, R., Waters, M.T., Scaffidi, A., Flematti, G.R., Smith, S.M., and Bond, C.S. (2013). The structure of the karrikin-insensitive protein (KAI2) in *Arabidopsis thaliana*. PLoS ONE **8:** e54758.

Capriotti, E., Fariselli, P., and Casadio, R. (2005). I-Mutant2.0: Predicting stability changes upon mutation from the protein sequence or structure. Nucleic Acids Res. **33:** W306–W310.

Challis, R.J., Hepworth, J., Mouchel, C., Waites, R., and Leyser, O. (2013). A role for more axillary growth1 (MAX1) in evolutionary diversity in strigolactone signaling upstream of MAX2. Plant Physiol. **161:** 1885–1902.

Clough, S.J., and Bent, A.F. (1998). Floral dip: A simplified method for Agrobacterium-mediated transformation of *Arabidopsis thaliana*. Plant J. **16:** 735–743.

Crawford, S., Shinohara, N., Sieberer, T., Williamson, L., George, G., Hepworth, J., Müller, D., Domagalska, M.A., and Leyser, O. (2010). Strigolactones enhance competition between shoot branches by dampening auxin transport. Development **137:** 2905–2913.

Czechowski, T., Stitt, M., Altmann, T., Udvardi, M.K., and Scheible, W.R. (2005). Genome-wide identification and testing of superior reference genes for transcript normalization in Arabidopsis. Plant Physiol. **139:** 5–17.

de Juan, D., Pazos, F., and Valencia, A. (2013). Emerging methods in protein co-evolution. Nat. Rev. Genet. **14:** 249–261.

Delaux, P.M., Xie, X., Timme, R.E., Puech-Pages, V., Dunand, C., Lecompte, E., Delwiche, C.F., Yoneyama, K., Bécard, G., and Séjalon-Delmas, N. (2012). Origin of strigolactones in the green lineage. New Phytol. **195:** 857–871.

Domagalska, M.A., and Leyser, O. (2011). Signal integration in the control of shoot branching. Nat. Rev. Mol. Cell Biol. **12:** 211–221.

Drummond, R.S., Martínez-Sánchez, N.M., Janssen, B.J., Templeton, K.R., Simons, J.L., Quinn, B.D., Karunairetnam, S., and Snowden, K.C. (2009). *Petunia hybrida* CAROTENOID CLEAVAGE DIOXYGENASE7 is involved in the production of negative and positive branching signals in petunia. Plant Physiol. **151:** 1867–1877.

Drummond, R.S., Sheehan, H., Simons, J.L., Martínez-Sánchez, N.M., Turner, R.M., Putterill, J., and Snowden, K.C. (2011). The expression of petunia strigolactone pathway genes is altered as part of the endogenous developmental program. Front. Plant Sci. **2:** 115.

Dun, E.A., Brewer, P.B., and Beveridge, C.A. (2009). Strigolactones: Discovery of the elusive shoot branching hormone. Trends Plant Sci. **14:** 364–372.

Dun, E.A., de Saint Germain, A., Rameau, C., and Beveridge, C.A. (2012). Antagonistic action of strigolactone and cytokinin in bud outgrowth control. Plant Physiol. **158:** 487–498.

Dun, E.A., de Saint Germain, A., Rameau, C., and Beveridge, C.A. (2013). Dynamics of strigolactone function and shoot branching responses in *Pisum sativum*. Mol. Plant **6:** 128–140.

Edgar, R.C. (2004). MUSCLE: A multiple sequence alignment method with reduced time and space complexity. BMC Bioinformatics **5:** 113.

Finlayson, S.A. (2007). Arabidopsis Teosinte Branched1-like 1 regulates axillary bud outgrowth and is homologous to monocot Teosinte Branched1. Plant Cell Physiol. **48:** 667–677.

Foo, E., Bullier, E., Goussot, M., Foucher, F., Rameau, C., and Beveridge, C.A. (2005). The branching gene RAMOSUS1 mediates interactions among two novel signals and auxin in pea. Plant Cell **17:** 464–474.

Foo, E., Turnbull, C.G., and Beveridge, C.A. (2001). Long-distance signaling and the control of branching in the rms1 mutant of pea. Plant Physiol. **126:** 203–209.

Gaiji, N., Cardinale, F., Prandi, C., Bonfante, P., and Ranghino, G. (2012). The computational-based structure of Dwarf14 provides evidence for its role as potential strigolactone receptor in plants. BMC Res. Notes **5:** 307.

Gao, Z., Qian, Q., Liu, X., Yan, M., Feng, Q., Dong, G., Liu, J., and Han, B. (2009). Dwarf 88, a novel putative esterase gene affecting architecture of rice plant. Plant Mol. Biol. **71:** 265–276.

Gomez-Roldan, V., et al. (2008). Strigolactone inhibition of shoot branching. Nature **455:** 189–194.

González-Grandío, E., Poza-Carrión, C., Sorzano, C.O., and Cubas, P. (2013). BRANCHED1 promotes axillary bud dormancy in response to shade in *Arabidopsis*. Plant Cell **25:** 834–850.

Guan, J.C., Koch, K.E., Suzuki, M., Wu, S., Latshaw, S., Petruff, T., Goulet, C., Klee, H.J., and McCarty, D.R. (2012). Diverse roles of strigolactone signaling in maize architecture and the uncoupling of a branching-specific subnetwork. Plant Physiol. **160:** 1303–1317.

Guo, S., Xu, Y., Liu, H., Mao, Z., Zhang, C., Ma, Y., Zhang, Q., Meng, Z., and Chong, K. (2013a). The interaction between OsMADS57 and OsTB1 modulates rice tillering via DWARF14. Nat. Commun. **4:** 1566.

Guo, Y., Zheng, Z., La Clair, J.J., Chory, J., and Noel, J.P. (2013b). Smoke-derived karrikin perception by the α/β-hydrolase KAI2 from Arabidopsis. Proc. Natl. Acad. Sci. USA **110:** 8284–8289.

Hamiaux, C., Drummond, R.S., Janssen, B.J., Ledger, S.E., Cooney, J.M., Newcomb, R.D., and Snowden, K.C. (2012). DAD2 is an α/β hydrolase likely to be involved in the perception of the plant branching hormone, strigolactone. Curr. Biol. **22:** 2032–2036.

Hayward, A., Stirnberg, P., Beveridge, C., and Leyser, O. (2009). Interactions between auxin and strigolactone in shoot branching control. Plant Physiol. **151:** 400–412.

Horton, P., Park, K.J., Obayashi, T., Fujita, N., Harada, H., Adams-Collier, C.J., and Nakai, K. (2007). WoLF PSORT: Protein localization predictor. Nucleic Acids Res. **35:** W585–W587.

Ishikawa, S., Maekawa, M., Arite, T., Onishi, K., Takamure, I., and Kyozuka, J. (2005). Suppression of tiller bud activity in tillering dwarf mutants of rice. Plant Cell Physiol. **46:** 79–86.

Jiang, L., et al. (2013). DWARF 53 acts as a repressor of strigolactone signalling in rice. Nature **504:** 401–405.

Johnson, X., Brcich, T., Dun, E.A., Goussot, M., Haurogné, K., Beveridge, C.A., and Rameau, C. (2006). Branching genes are conserved across species. Genes controlling a novel signal in pea are coregulated by other long-distance signals. Plant Physiol. **142:** 1014–1026.

Kagiyama, M., Hirano, Y., Mori, T., Kim, S.Y., Kyozuka, J., Seto, Y., Yamaguchi, S., and Hakoshima, T. (2013). Structures of D14 and D14L in the strigolactone and karrikin signaling pathways. Genes Cells **18:** 147–160.

Kohlen, W., Charnikhova, T., Liu, Q., Bours, R., Domagalska, M.A., Beguerie, S., Verstappen, F., Leyser, O., Bouwmeester, H., and Ruyter-Spira, C. (2011). Strigolactones are transported through the xylem and play a key role in shoot architectural response to phosphate deficiency in nonarbuscular mycorrhizal host Arabidopsis. Plant Physiol. **155:** 974–987.

Kretzschmar, T., Kohlen, W., Sasse, J., Borghi, L., Schlegel, M., Bachelier, J.B., Reinhardt, D., Bours, R., Bouwmeester, H.J., and Martinoia, E. (2012). A petunia ABC protein controls strigolactone-dependent symbiotic signalling and branching. Nature **483:** 341–344.

Lin, H., Wang, R., Qian, Q., Yan, M., Meng, X., Fu, Z., Yan, C., Jiang, B., Su, Z., Li, J., and Wang, Y. (2009). DWARF27, an iron-containing protein required for the biosynthesis of strigolactones, regulates rice tiller bud outgrowth. Plant Cell **21:** 1512–1525.

Liu, W., Wu, C., Fu, Y., Hu, G., Si, H., Zhu, L., Luan, W., He, Z., and Sun, Z. (2009). Identification and characterization of HTD2: A novel gene negatively regulating tiller bud outgrowth in rice. Planta **230:** 649–658.

Martín-Trillo, M., and Cubas, P. (2010). TCP genes: A family snapshot ten years later. Trends Plant Sci. **15:** 31–39.

Martín-Trillo, M., Grandío, E.G., Serra, F., Marcel, F., Rodríguez-Buey, M.L., Schmitz, G., Theres, K., Bendahmane, A., Dopazo, H., and Cubas, P. (2011). Role of tomato BRANCHED1-like genes in the control of shoot branching. Plant J. **67:** 701–714.

Mashiguchi, K., Sasaki, E., Shimada, Y., Nagae, M., Ueno, K., Nakano, T., Yoneyama, K., Suzuki, Y., and Asami, T. (2009). Feedback-regulation of strigolactone biosynthetic genes and strigolactone-regulated genes in Arabidopsis. Biosci. Biotechnol. Biochem. **73:** 2460–2465.

Minakuchi, K., Kameoka, H., Yasuno, N., Umehara, M., Luo, L., Kobayashi, K., Hanada, A., Ueno, K., Asami, T., Yamaguchi, S., and Kyozuka, J. (2010). FINE CULM1 (FC1) works downstream of strigolactones to inhibit the outgrowth of axillary buds in rice. Plant Cell Physiol **7:** 1127–1135.

Murase, K., Hirano, Y., Sun, T.P., and Hakoshima, T. (2008). Gibberellin-induced DELLA recognition by the gibberellin receptor GID1. Nature **456:** 459–463.

Muth, T., García-Martín, J.A., Rausell, A., Juan, D., Valencia, A., and Pazos, F. (2012). JDet: Interactive calculation and visualization of function-related conservation patterns in multiple sequence alignments and structures. Bioinformatics **28:** 584–586.

Nakagawa, T., Kurose, T., Hino, T., Tanaka, K., Kawamukai, M., Niwa, Y., Toyooka, K., Matsuoka, K., Jinbo, T., and Kimura, T. (2007). Development of series of gateway binary vectors, pGWBs, for realizing efficient construction of fusion genes for plant transformation. J. Biosci. Bioeng. **104:** 34–41.

Nakamura, H., et al. (2013). Molecular mechanism of strigolactone perception by DWARF14. Nat. Commun. **4:** 2613.

Nelson, D.C., Scaffidi, A., Dun, E.A., Waters, M.T., Flematti, G.R., Dixon, K.W., Beveridge, C.A., Ghisalberti, E.L., and Smith, S.M. (2011). F-box protein MAX2 has dual roles in karrikin and strigolactone signaling in *Arabidopsis thaliana*. Proc. Natl. Acad. Sci. USA **108:** 8897–8902.

Niwa, M., Daimon, Y., Kurotani, K., Higo, A., Pruneda-Paz, J.L., Breton, G., Mitsuda, N., Kay, S.A., Ohme-Takagi, M., Endo, M., and Araki, T. (2013). BRANCHED1 interacts with FLOWERING LOCUS T to repress the floral transition of the axillary meristems in *Arabidopsis*. Plant Cell **25:** 1228–1242.

Nordström, A., Tarkowski, P., Tarkowska, D., Norbaek, R., Astot, C., Dolezal, K., and Sandberg, G. (2004). Auxin regulation of cytokinin biosynthesis in *Arabidopsis thaliana*: A factor of potential importance for auxin-cytokinin-regulated development. Proc. Natl. Acad. Sci. USA **101:** 8039–8044.

Pasare, S.A., Ducreux, L.J., Morris, W.L., Campbell, R., Sharma, S.K., Roumeliotis, E., Kohlen, W., van der Krol, S., Bramley, P. M., Roberts, A.G., Fraser, P.D., and Taylor, M.A. (2013). The role of the potato (*Solanum tuberosum*) CCD8 gene in stolon and tuber development. New Phytol. **198:** 1108–1120.

Ponce, M.R., Robles, P., and Micol, J.L. (1999). High-throughput genetic mapping in *Arabidopsis thaliana*. Mol. Gen. Genet. **261:** 408–415.

Ponce, M.R., Robles, P., Lozano, F.M., Brotóns, M.A., and Micol, J.L. (2006). Low-resolution mapping of untagged mutations. Methods Mol. Biol. **323:** 105–113.

Prusinkiewicz, P., Crawford, S., Smith, R.S., Ljung, K., Bennett, T., Ongaro, V., and Leyser, O. (2009). Control of bud activation by an auxin transport switch. Proc. Natl. Acad. Sci. USA **106:** 17431–17436.

Ragni, L., Nieminen, K., Pacheco-Villalobos, D., Sibout, R., Schwechheimer, C., and Hardtke, C.S. (2011). Mobile gibberellin directly stimulates *Arabidopsis* hypocotyl xylem expansion. Plant Cell **23:** 1322–1336.

Rausell, A., Juan, D., Pazos, F., and Valencia, A. (2010). Protein interactions and ligand binding: From protein subfamilies to functional specificity. Proc. Natl. Acad. Sci. USA **107:** 1995–2000.

Schymkowitz, J., Borg, J., Stricher, F., Nys, R., Rousseau, F., and Serrano, L. (2005). The FoldX web server: An online force field. Nucleic Acids Res. **33:** W382–W388.

Sessions, A., Weigel, D., and Yanofsky, M.F. (1999). The *Arabidopsis thaliana* MERISTEM LAYER 1 promoter specifies epidermal expression in meristems and young primordia. Plant J. **20:** 259–263.

Seto, Y., Sado, A., Asami, K., Hanada, A., Umehara, M., Akiyama, K., and Yamaguchi, S. (2014). Carlactone is an endogenous biosynthetic precursor for strigolactones. Proc. Natl. Acad. Sci USA **11:** 1640–1645.

Shen, H., Luong, P., and Huq, E. (2007). The F-box protein MAX2 functions as a positive regulator of photomorphogenesis in Arabidopsis. Plant Physiol. **145:** 1471–1483.

Shimada, A., Ueguchi-Tanaka, M., Nakatsu, T., Nakajima, M., Naoe, Y., Ohmiya, H., Kato, H., and Matsuoka, M. (2008). Structural basis for gibberellin recognition by its receptor GID1. Nature **456:** 520–523.

Shinohara, N., Taylor, C., and Leyser, O. (2013). Strigolactone can promote or inhibit shoot branching by triggering rapid depletion of the auxin efflux protein PIN1 from the plasma membrane. PLoS Biol. **11:** e1001474.

Simons, J.L., Napoli, C.A., Janssen, B.J., Plummer, K.M., and Snowden, K.C. (2007). Analysis of the DECREASED APICAL DOMINANCE genes of petunia in the control of axillary branching. Plant Physiol. **143:** 697–706.

Skoog, F., and Thimann, K.V. (1934). Further experiments on the inhibition of the development of lateral buds by growth hormone. Proc. Natl. Acad. Sci. USA **20:** 480–485.

Snowden, K.C., Simkin, A.J., Janssen, B.J., Templeton, K.R., Loucas, H.M., Simons, J.L., Karunairetnam, S., Gleave, A.P., Clark, D.G., and Klee, H.J. (2005). The Decreased apical dominance1/*Petunia hybrida* CAROTENOID CLEAVAGE DIOXYGENASE8 gene affects branch production and plays a role in leaf senescence, root growth, and flower development. Plant Cell **17:** 746–759.

Sorefan, K., Booker, J., Haurogné, K., Goussot, M., Bainbridge, K., Foo, E., Chatfield, S., Ward, S., Beveridge, C., Rameau, C., and Leyser, O. (2003). MAX4 and RMS1 are orthologous dioxygenase-like genes that regulate shoot branching in Arabidopsis and pea. Genes Dev. **17:** 1469–1474.

Stirnberg, P., Furner, I.J., and Ottoline Leyser, H.M. (2007). MAX2 participates in an SCF complex which acts locally at the node to suppress shoot branching. Plant J. **50:** 80–94.

Stirnberg, P., van De Sande, K., and Leyser, H.M. (2002). MAX1 and MAX2 control shoot lateral branching in Arabidopsis. Development **129:** 1131–1141.

Thimann, K.V., and Skoog, F. (1933). Studies on the growth hormone of plants: III. The inhibiting action of the growth substance on bud development. Proc. Natl. Acad. Sci. USA **19:** 714–716.

Umehara, M., Hanada, A., Yoshida, S., Akiyama, K., Arite, T., Takeda-Kamiya, N., Magome, H., Kamiya, Y., Shirasu, K., Yoneyama, K., Kyozuka, J., and Yamaguchi, S. (2008). Inhibition of shoot branching by new terpenoid plant hormones. Nature **455:** 195–200.

Wang, Y., Sun, S., Zhu, W., Jia, K., Yang, H., and Wang, X. (2013). Strigolactone/MAX2-induced degradation of brassinosteroid transcriptional effector BES1 regulates shoot branching. Dev. Cell **27:** 681–688.

Waters, M.T., and Smith, S.M. (2013). KAI2- and MAX2-mediated responses to karrikins and strigolactones are largely independent of HY5 in Arabidopsis seedlings. Mol. Plant **6:** 63–75.

Waters, M.T., Brewer, P.B., Bussell, J.D., Smith, S.M., and Beveridge, C.A. (2012a). The Arabidopsis ortholog of rice DWARF27 acts upstream of MAX1 in the control of plant development by strigolactones. Plant Physiol. **159:** 1073–1085.

Waters, M.T., Nelson, D.C., Scaffidi, A., Flematti, G.R., Sun, Y.K., Dixon, K.W., and Smith, S.M. (2012b). Specialisation within the

DWARF14 protein family confers distinct responses to karrikins and strigolactones in Arabidopsis. Development **139:** 1285–1295.

Waters, M.T., Scaffidi, A., Flematti, G.R., and Smith, S.M. (2013). The origins and mechanisms of karrikin signalling. Curr. Opin. Plant Biol. **16:** 667–673.

Worth, C.L., Preissner, R., and Blundell, T.L. (2011). SDM—A server for predicting effects of mutations on protein stability and malfunction. Nucleic Acids Res. **39:** W215–W222.

Ye, Y., and Godzik, A. (2004). FATCAT: A web server for flexible structure comparison and structure similarity searching. Nucleic Acids Res. **32:** W582–W585.

Yin, S., Ding, F., and Dokholyan, N.V. (2007). Eris: An automated estimator of protein stability. Nat. Methods **4:** 466–467.

Yu, J.W., et al. (2008). COP1 and ELF3 control circadian function and photoperiodic flowering by regulating GI stability. Mol. Cell **32:** 617–630.

Zhao, L.H., et al. (2013). Crystal structures of two phytohormone signal-transducing α/β hydrolases: Karrikin-signaling KAI2 and strigolactone-signaling DWARF14. Cell Res. **23:** 436–439.

Zhou, F., et al. (2013). D14-SCF(D3)-dependent degradation of D53 regulates strigolactone signalling. Nature **504:** 406–410.

Zou, J., Zhang, S., Zhang, W., Li, G., Chen, Z., Zhai, W., Zhao, X., Pan, X., Xie, Q., and Zhu, L. (2006). The rice HIGH-TILLERING DWARF1 encoding an ortholog of Arabidopsis MAX3 is required for negative regulation of the outgrowth of axillary buds. Plant J. **48:** 687–698.